SOUTHWEST RESEARCH INSTITUTE
8500 Culebra Road, San Antonio, Texas 78206

Department of Mechanical Sciences

A STUDY OF JOINT DISCONTINUITY IN VIBRATIONS OF COMPOSITE SHELLS

by

William C. L. Hu

Technical Report No. 6
Contract NASr-94(06)
SwRI Project No. 02-1504

Prepared for

National Aeronautics and Space Administration
Washington 25, D. C.

May 12, 1966

APPROVED BY:

H. Norman Abramson, Director
Department of Mechanical Sciences

ABSTRACT

The vibrational characteristics of composite (cone-cylinder) shells are investigated analytically and experimentally. The behavior of the circular joint connecting the conical and the cylindrical shell components is discussed in detail. Both the analysis and the experimental results reveal that the derivatives of the mode functions are discontinuous at the joint, where a V-shaped minimum of normal displacement was observed in all modes being excited. It is evident that dynamic stress concentration is involved even in free vibrations of such shell structures. The jump conditions are formulated for the cone-cylinder joint, and various approaches of solving this problem are discussed.

TABLE OF CONTENTS

LIST OF ILLUSTRATIONS

NOMENCLATURE

a	radius of the cylindrical shell
C	$= Eh/(1 - \nu^2)$, extensional modulus
D	$= Eh^3/12(1 - \nu^2)$, flexural modulus
E	Young's modulus
h	thickness of shell
L	length of the cylindrical component
$M_s, M_\theta, M_{s\theta}$	stress couple resultants
$N_s, N_\theta, N_{s\theta}$	stress resultants
m	axial mode number
n	circumferential wave number
Q_s, Q_θ	transverse shearing stress resultants
R_1, R_2	principal radii of curvature
r	cylindrical coordinate, radial direction
s	distance along meridian of shell
t	time
u, v, w	displacements of shell
z	cylindrical coordinate, axial direction
α	semivertex angle of cone
β_s, β_θ	angular displacement of shell normal
θ	circumferential coordinate angle
κ	shear constant

κ_1	$= 1/R_1$ curvature
ν	Poisson's ratio
ρ	mass density of shell
ϕ	colatitude angle
ω	natural frequency in rad/sec

INTRODUCTION

In the existing literature on vibrations of elastic shells, abundant information has been accumulated on the vibrational characteristics for elementary shell configurations. Recent surveys[1, 2, 3*] indicate that, with but a few exceptions, these previous investigations have been exclusively dealing with thin shells of revolution with simple, analytical meridian curves, of which the cylindrical, spherical, and conical shells have received by far the most attention. Although a few investigators have developed general finite-difference[4] or numerical integration[5, 6] techniques which allow the calculation of the natural frequencies and mode functions of arbitrary shells of revolution, no specific discussion, however, is available concerning vibrations of a composite shell whose meridian contains a geometric or material discontinuity. The present investigation is intended to provide preliminary information of the boundary-layer effects of such discontinuities when the composite shell is in vibration.

Contradictory to what some previous authors have expected (e.g., Ref. 7), when a composite shell is vibrating at one of its resonant frequencies, the mode shape in the meridional direction is not, as a rule, given by a smooth curve. On the contrary, the derivatives of all displacement functions (including the slope of normal displacement, $\partial w/\partial s$) may be shown to be discontinuous across the joint. This is both an analytical

*Superscripts refer to references cited at the end of this report.

deduction from elastic shell theory, and an actual observation from the mode-shape mapping in the present experiments on two composite (cone-cylinder) shell models, in which a V-shaped minimum of normal displacement w was observed in all normal modes being excited.

An important consequence of this boundary-layer phenomenon is the large dynamic stresses induced in the neighborhood of the joint. The extremely sharp curvature change observed near the joint indicates that the shell material may suffer local plastic deformation even when the vibration amplitude is relatively small. The vibratory nature of the local bending stresses may easily lead to material fatigue or fracture and thus requires special attention in the analysis and design of such composite shell structures.

ANALYSIS

Discontinuities at Joints

Before we examine the vibrational characteristics of a specific composite (cone-cylinder) shell, it is expedient to classify the different types of discontinuities possible at the joints of composite shells of revolution, and discuss their effects on stresses and deformations. Let (r, θ, z) be the reference cylindrical coordinates, where z coincides with the axis of symmetry of the shell, then the meridian curve of the mid-surface may be represented by the parametric equations

$$r = r(s) \quad , \quad z = z(s) \tag{1}$$

where s is the arc length measured along the meridian. The principal radii of curvature are

$$R_1 = (r'^2 + z'^2)^{3/2} \Big/ (r'z'' - r''z')$$
$$R_2 = r/\sin\phi \tag{2}$$

where prime denotes differentiation with respect to the argument s, and ϕ is the colatitude angle between a normal and the z-axis,

$$\phi = \tan^{-1}(z'/r') \tag{3}$$

For a composite shell, r and z are continuous functions of s, but their derivatives may be discontinuous at the joint $s = s_{jt}$.

Referring to the curvilinear coordinates (s, θ), a first-order shell theory gives the following set of equations governing the free vibrations of shells of revolution. These consist of five equations of motion,

$$
\begin{aligned}
&rN_{s,s} + N_{s\theta,\theta} + (N_s - N_\theta)\cos\phi + rQ_s/R_1 = \rho h r u_{,tt} \\
&rN_{s\theta,s} + N_{\theta,\theta} + 2N_{s\theta}\cos\phi + Q_\theta \sin\phi = \rho h r v_{,tt} \\
&rQ_{s,s} + Q_{\theta,\theta} + Q_s \cos\phi - rN_s/R_1 - N_\theta \sin\phi = \rho h r w_{,tt} \qquad (4) \\
&rM_{s,s} + M_{s\theta,\theta} + (M_s - M_\theta)\cos\phi - rQ_s = (\rho h^3/12) r\beta_{s,tt} \\
&rM_{s\theta,s} + M_{\theta,\theta} + 2M_{s\theta}\cos\phi - rQ_\theta = (\rho h^3/12) r\beta_{\theta,tt}
\end{aligned}
$$

and eight constitutive equations,

$$
\begin{aligned}
N_s &= C[(u_{,s} + w/R_1) + (\nu/r)(v_{,\theta} + u\cos\phi + w\sin\phi)] \\
N_\theta &= C[r^{-1}(v_{,\theta} + u\cos\phi + w\sin\phi) + \nu(u_{,s} + w/R_1)] \\
N_{s\theta} &= \frac{1-\nu}{2} C[v_{,s} + r^{-1}(u_{,\theta} - v\cos\phi)] \\
M_s &= D[\beta_{s,s} + (\nu/r)(\beta_{\theta,\theta} + \beta_s\cos\phi)] \qquad (5) \\
M_\theta &= D[r^{-1}(\beta_{\theta,\theta} + \beta_s\cos\phi) + \nu\beta_{s,s}] \\
M_{s\theta} &= \frac{1-\nu}{2} D[\beta_{\theta,s} + r^{-1}(\beta_{s,\theta} - \beta_\theta\cos\phi)] \\
Q_s &= \frac{1-\nu}{2} C\kappa[\beta_s + w_{,s} - u/R_1] \\
Q_\theta &= \frac{1-\nu}{2} C\kappa[\beta_\theta + r^{-1}(w_{,\theta} - v\sin\phi)]
\end{aligned}
$$

in which subscripts following comma denote partial differentiation with respect to the subscript variables, $C = Eh/(1 - \nu^2)$ is the extensional modulus, $D = Eh^3/12(1 - \nu^2)$ the flexural modulus, and other notations are those commonly used in shell theory. From an examination of the parameters entering into the governing Eqs. (4) and (5), we can classify the possible joint discontinuities into the following categories:

I. Geometric Discontinuities

(a) Joints where R_1 is discontinuous. A familiar example of this type is furnished by the joint connecting a hemispherical bulkhead to a cylindrical shell.

(b) Joints where ϕ, or equivalently, R_2 is discontinuous. The joint connecting a conical shell to a cylindrical shell, as discussed below, is an example. This type of joint has a much stronger discontinuity and, as will be seen, may suppress local deflection like a stiffening ring.

(c) Joints where the thickness h has an abrupt change. If the difference in thickness is sufficiently large, say a ratio of ten to one, then the thinner shell may be considered clamped at the joint.

II. Material Discontinuities

Joints of two shell components made of different materials, so that the elastic modulus E and Poisson's ratio ν change abruptly.

It is evident that, in an actual joint, two or more types of discontinuities listed above may be present together. In any case, the conditions that must be satisfied by the ten fundamental shell variables (eight if classical shell theory is employed) at the joint can be put into the following general form:

$$u^- \cos\phi^- + w^- \sin\phi^- = u^+ \cos\phi^+ + w^+ \sin\phi^+,$$

$$u^- \sin\phi^- - w^- \cos\phi^- = u^+ \sin\phi^+ - w^+ \cos\phi^+, \tag{6}$$

$$v^- = v^+ \quad , \quad \beta_s^- = \beta_s^+ \quad , \quad \beta_\theta^- = \beta_\theta^+;$$

$$N_s^- \cos\phi^- + Q_s^- \sin\phi^- = N_s^+ \cos\phi^+ + Q_s^+ \sin\phi^+,$$

$$N_s^- \sin\phi^- - Q_s^- \cos\phi^- = N_s^+ \sin\phi^+ - Q_s^+ \cos\phi^+, \tag{7}$$

$$N_{s\theta}^- = N_{s\theta}^+ \quad , \quad M_s^- = M_s^+ \quad , \quad M_{s\theta}^- = M_{s\theta}^+$$

in which the superscript "-" denotes the value at one side of the joint, $s = s_{jt} - 0$, while "+" the value at the other side of the joint, $s = s_{jt} + 0$. It is seen that the first five conditions, (6), ensure the compatibility of the displacement field so that no cracks exist, and the remaining five conditions, (7), are merely Newton's third law that action equals reaction. If we introduce (5) into (7) and make use of (6) to cancel some equal terms, we can in general obtain a set of "jump conditions" for each type of discontinuity. For example, if the joint is of type I(a) and the known discontinuity in curvature is given by

$$\Delta\kappa_1 = \frac{1}{R_1^+} - \frac{1}{R_1^-} \tag{8}$$

then the conditions (6) become simply

$$\left\{u^-, v^-, w^-, \beta_s^-, \beta_\theta^-\right\} = \left\{u^+, v^+, w^+, \beta_s^+, \beta_\theta^+\right\} \tag{9}$$

and the jump conditions obtained from (7), simplified with the help of (9), may be shown as:

$$\Delta u_{,s} \equiv u^{+}_{,s} - u^{-}_{,s} = - w^{-}\Delta\kappa_1$$

$$\Delta w_{,s} \equiv w^{+}_{,s} - w^{-}_{,s} = u^{-}\Delta\kappa_1 \qquad (10)$$

$$\Delta v_{,s} = \Delta\beta_{s,s} = \Delta\beta_{\theta,s} = 0$$

Therefore, the displacements u and w are continuous functions of s with only piecewise continuous derivatives*, while v, β_s and β_θ have continuous first derivatives.

Aside from the discontinuity at the joint line, the solution of the free vibration problem of axisymmetric composite shells may proceed similarly to that of simple shells. For a normal-mode vibration, the shell variables have the usual form

$$\begin{Bmatrix} u,\ w,\ \beta_s \\ N_s,\ N_\theta,\ Q_s \\ M_s,\ M_\theta \end{Bmatrix} = \begin{Bmatrix} u_n,\ w_n,\ \beta_{sn} \\ N_{sn},\ N_{\theta n},\ Q_{sn} \\ M_{sn},\ M_{\theta n} \end{Bmatrix} \sin n\theta \cos \omega t \qquad (11)$$

$$\begin{Bmatrix} v,\ \beta_\theta \\ N_{s\theta},\ Q_\theta \\ M_{s\theta} \end{Bmatrix} = \begin{Bmatrix} v_n,\ \beta_{\theta n} \\ N_{s\theta n},\ Q_{\theta n} \\ M_{s\theta n} \end{Bmatrix} \cos n\theta \cos \omega t$$

where ω is a natural frequency and n an integer representing the circumferential wave number; however, the mode functions with subscript n are no longer smooth functions of s as in the case of simple shells.

*If we impose the continuity of the slope $w_{,s}$, the stress conditions (7) will be violated paradoxically.

Vibrations of Composite Conic-Cylindrical Shells

The geometry of the composite shell to be considered is defined in Figure 1. Let α denote the semivertex angle of the truncated conical shell component, which extends from $s = s_1$ to $s = s_2$, s being measured from the vertex. At the major edge s_2, it is joined to a cylindrical shell with radius $a = s_2 \sin\alpha$, and length L. The meridian is thus given by the broken line,

$$\begin{aligned} r(s) &= s \sin\alpha \quad , \quad s_1 \le s \le s_2 \\ r(s) &= a \quad , \quad s_2 \le s \le s_2 + L \end{aligned} \tag{12}$$

and the colatitude angle ϕ is constant in each component,

$$\begin{aligned} \phi = \phi^- &= \pi/2 - \alpha \quad , \quad s_1 \le s < s_2 \\ \phi = \phi^+ &= \pi/2 \quad , \quad s_2 < s \le s_2 + L \end{aligned} \tag{13}$$

Therefore, the joint belongs to type I(b), with the given discontinuity

$$\Delta\phi = \phi^+ - \phi^- = \alpha$$

The governing shell equations may be obtained by using (12) and (13) in (4) and (5). The conditions (6) now may be written

$$\begin{aligned} &u^- \sin\alpha + w^- \cos\alpha = w^+, \\ &u^- \cos\alpha - w^- \sin\alpha = u^+, \\ &v^- = v^+ \ , \ \beta_s^- = \beta_s^+ \ , \ \beta_\theta^- = \beta_\theta^+, \end{aligned} \tag{14}$$

and, similarly, the conditions (7) become:

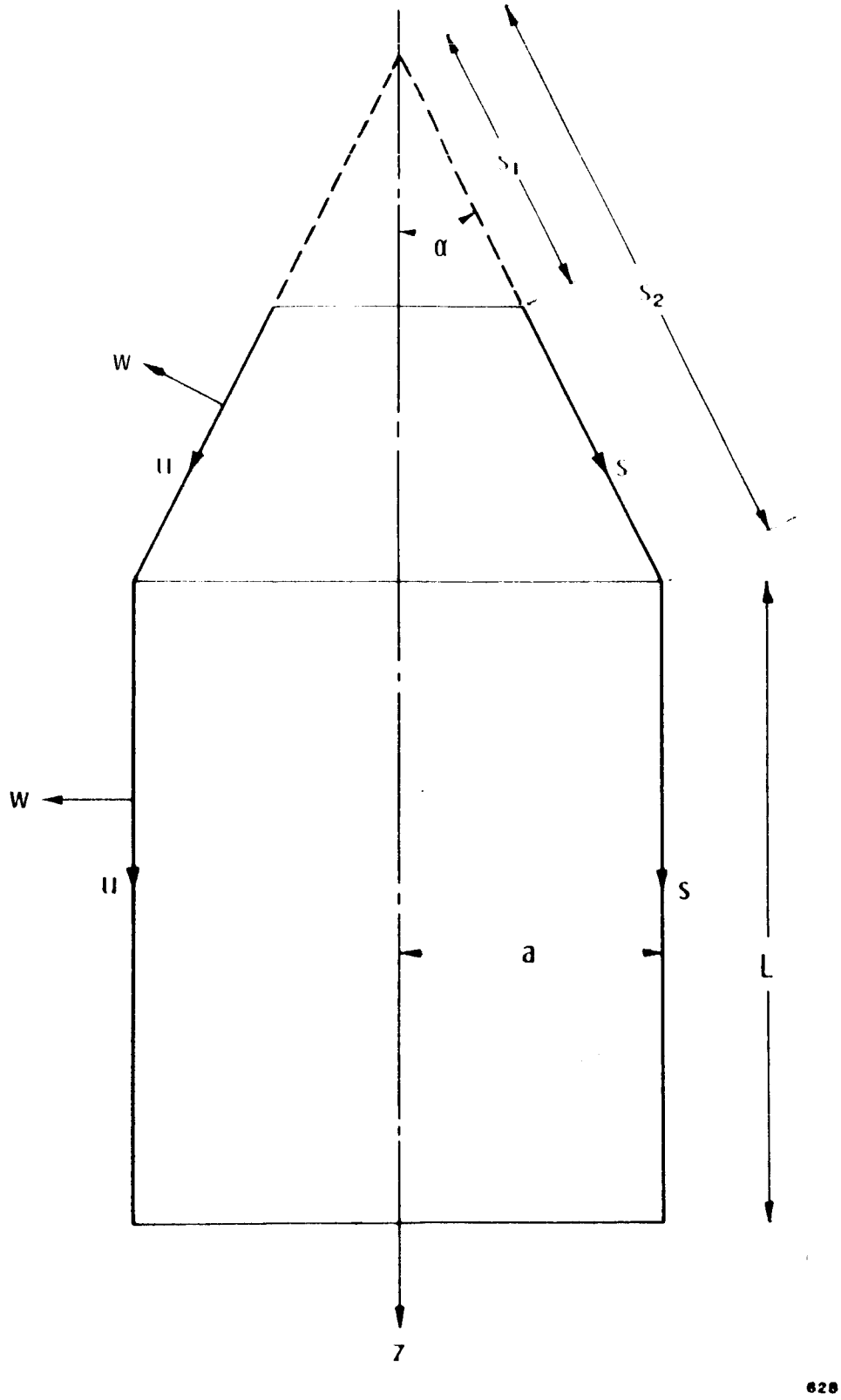

Figure 1. Geometry and Notation

$$N_s^- \sin\alpha + Q_s^- \cos\alpha = Q_s^+,$$

$$N_s^- \cos\alpha - Q_s^- \sin\alpha = N_s^+, \tag{15}$$

$$N_{s\theta}^- = N_{s\theta}^+ , \quad M_s^- = M_s^+ , \quad M_{s\theta}^- = M_{s\theta}^+$$

To determine the jump condition of the derivatives of the displacements, we introduce the corresponding constitutive equations into (15), and simplify the result with the help of (14), to obtain

$$w_{,s}^+ = w_{,s}^- \cos\alpha - \beta_s^- (1 - \cos\alpha) + \frac{2\sin\alpha}{(1-\nu)\kappa}\left[u_{,s}^- + \frac{\nu}{a}(v_{,\theta}^- + u^- \sin\alpha + w^- \cos\alpha)\right]$$

$$u_{,s}^+ = u_{,s}^- \cos\alpha - \frac{\nu}{a}(v_{,\theta}^- + u^- \sin\alpha + w^- \cos\alpha)(1 - \cos\alpha) - \frac{1-\nu}{2}\kappa(\beta_s^- + w_{,s}^-)\sin\alpha$$

$$\Delta v_{,s} \equiv v_{,s}^+ - v_{,s}^- = \frac{1}{a}[u_{,\theta}^- (1 - \cos\alpha) + w_{,\theta}^- \sin\alpha - v^- \sin\alpha] \tag{16}$$

$$\Delta\beta_{s,s} \equiv \beta_{s,s}^+ - \beta_{s,s}^- = \frac{\nu}{a}\beta_s^- \sin\alpha$$

$$\Delta\beta_{\theta,s} \equiv \beta_{\theta,s}^+ - \beta_{\theta,s}^- = -\frac{1}{a}\beta_\theta^- \sin\alpha$$

From the first two equations above, it can be seen that the jump conditions for $w_{,s}$ and $u_{,s}$ are very complicated even within the scope of the first-order shell theory considered. This fact makes all analytical methods using equations in terms of displacement variables alone unsuitable for the solution of this problem. For example, the Fourier expansion method

used in Refs. 8 and 9 will not readily yield convergent results* because no proper account can be easily taken of the jump condition (16). Also, if finite-difference techniques are used to solve the governing differential equations in displacements, one will find that the finite-difference equations at the joint become extremely unwieldy due to the imposition of (16).

On the other hand, the numerical integration methods, such as the computer technique developed by Kalnins[5], can account for the joint conditions, (14) and (15), with relatively simple modification. In these methods, the first derivatives of the ten fundamental variables are directly integrated by numerical means, and the natural frequencies are determined by trial and error. Thus, when the numerical integration of the conical shell equations procceds from $s = s_1$ to the joint $s = s_2$, the conditions (14) and (15) are imposed to obtain a set of "initial values" of the ten fundamental variables, then the integration process may be carried on beyond the joint, using a consistent set of shell equations for the cylindrical shell component. Other details of this technique will not be discussed further here, since, besides the modification outlined above, the readers may be referred to Ref. 5. The degree of validity of these joint conditions, however, will be discussed further in the next section.

Physical Significance and the Boundary-Layer Stresses

The above analysis of the joint, treated as a line of discontinuity, provides a mathematical model of physical reality within linear elastic

*Note that the Fourier series expansion of piecewise smooth functions are not termwise differentiable twice.

shell theory which is similar to other singular quantities in mechanics such as concentrated force, line load, point source or sink, vortex street, etc. These concepts idealize the complicated but highly localized physical phenomenon and simplify the analytical solution of problems. To analyze the validity of this mathematical model, we will investigate a limiting process which has the cone-cylinder joint as its limit.

Consider that a transition zone at the joint is cut off and replaced by a toroidal shell adapter with small radius of curvature δR_1 as indicated in Fig. 2. The width of the toroidal segment would be $\alpha \cdot \delta R_1$. Note that the center of the meridional arc must fall on the bisector of the joint angle to allow a smooth transition. From the constitutive equations [Eq. (5)], we find that δR_1 appears at several places in the denominator of the coefficients. Therefore, the narrow toroidal segment is enormously stiffer than a neighboring strip in the conical or cylindrical shell due to the smallness of δR_1. When we take the limiting process of moving the center of the arc toward the corner, δR_1 will soon reach the same order of magnitudes as the shell thickness h, and thus shell theory ceases to apply. Meanwhile, several important features will be lost in the limiting process:

(1) The much greater bending stiffness of the toroidal segment, or the limiting ring with "L-cross section," cannot be retained in the analysis of the limit case. In the previous formulation of linear shell theory and joint conditions, the bending rigidity $D = Eh^3/12(1 - \nu^2)$ was used throughout the composite shell.

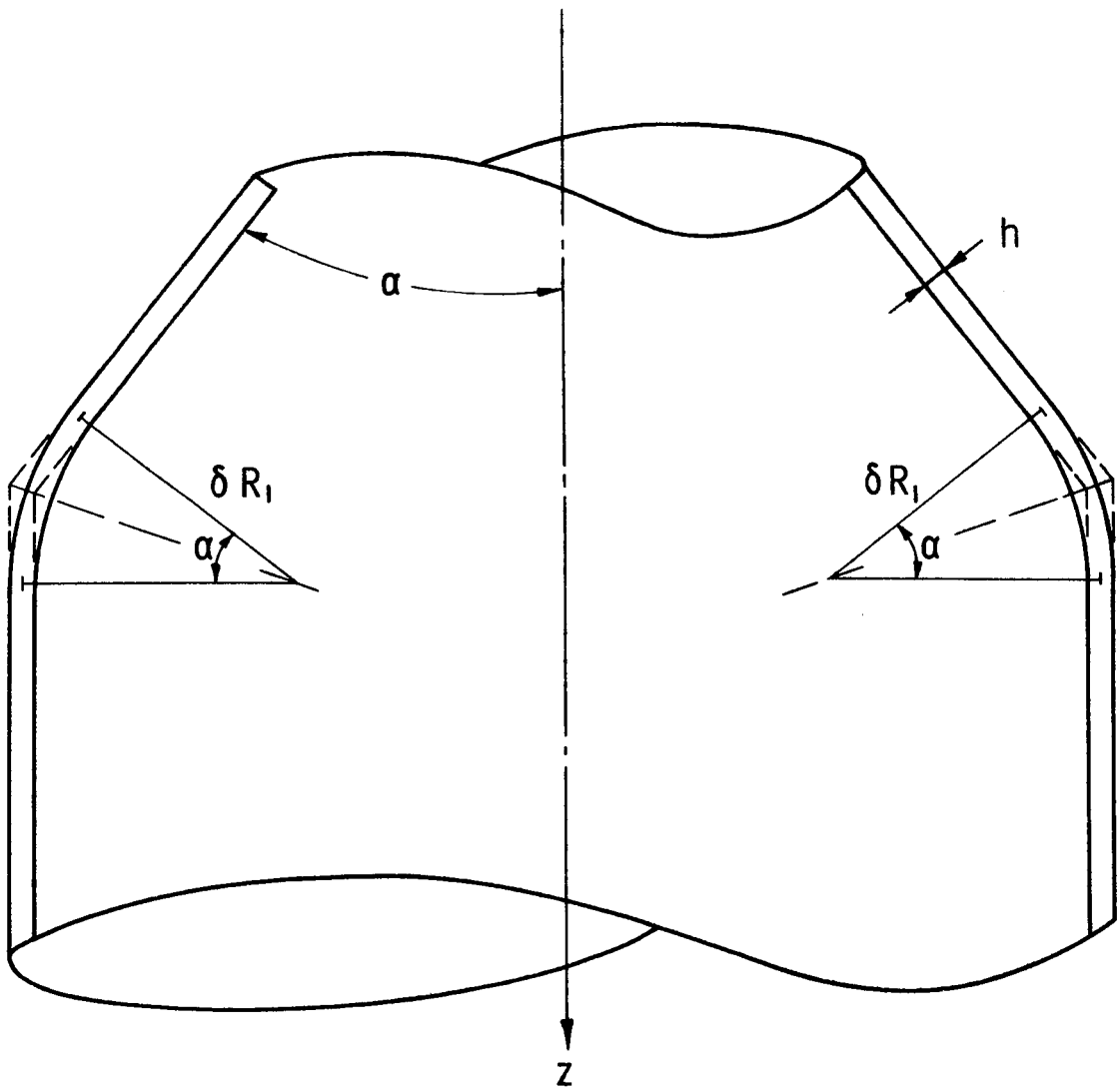

Figure 2. Transition Zone of a Cone-Cylinder Joint

(2) Due to this large bending stiffness of the "joint-ring" with L-cross section, the local lateral displacement w will be greatly suppressed, as will be seen later in the experimental mode shape plot. Therefore, the joint has the function of a ring stiffener, on which large transverse shearing loads $(Q^*_{sn})^-$ and $(Q^*_{sn})^+$, together with other loads, are exerted by the conical and cylindrical shell, respectively. A schematic drawing of a section of the "joint-ring" is shown in Fig. 3. This "ring-action" of the joint cannot be fully accounted for in the limit case of linear shell equations and joint conditions.

(3) If we examine the joint-ring separately (Fig. 3), we can assert that the loads $(Q^*_{sn})^-$ and $(Q^*_{sn})^+$ will be supported jointly by the bending stress, $M_{\theta n}$, and the hoop stress, $N_{\theta n}$, within the L-cross section. Therefore, the local membrane stresses are also profoundly affected by the "ring-action," although the membrane stiffness has no apparent increase at the joint.

In short, the mathematical discontinuity or the physical "ring-action" at the cone-cylinder joint creates a system of boundary-layer stresses superposed on the stress field predicted by the linear shell theory and joint conditions. From the qualitative analysis of the ring-action given above, some general understanding can be obtained. A few important boundary-layer stresses are shown qualitatively in Fig. 4.

In this connection, we conclude that even if we can solve the system of elastic shell equations, (4) and (5), together with prescribed boundary conditions and the joint conditions (14) and (15), with high accuracy (say, by a modified Kalnins' numerical integration technique[5]), the results will still be only an approximate solution to this problem. Although some boundary-layer shell theories are discussed in the literature, to the author's knowledge, they are not readily applicable to the solution of this composite

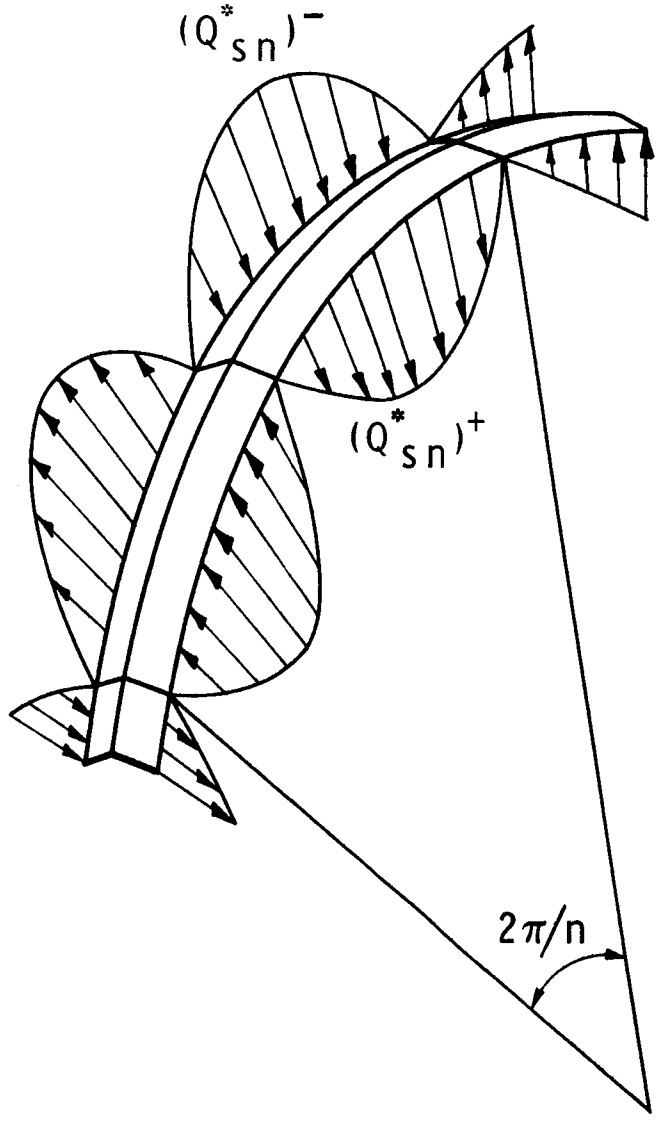

Figure 3. Schematic of the Loads on the "Joint-Ring"

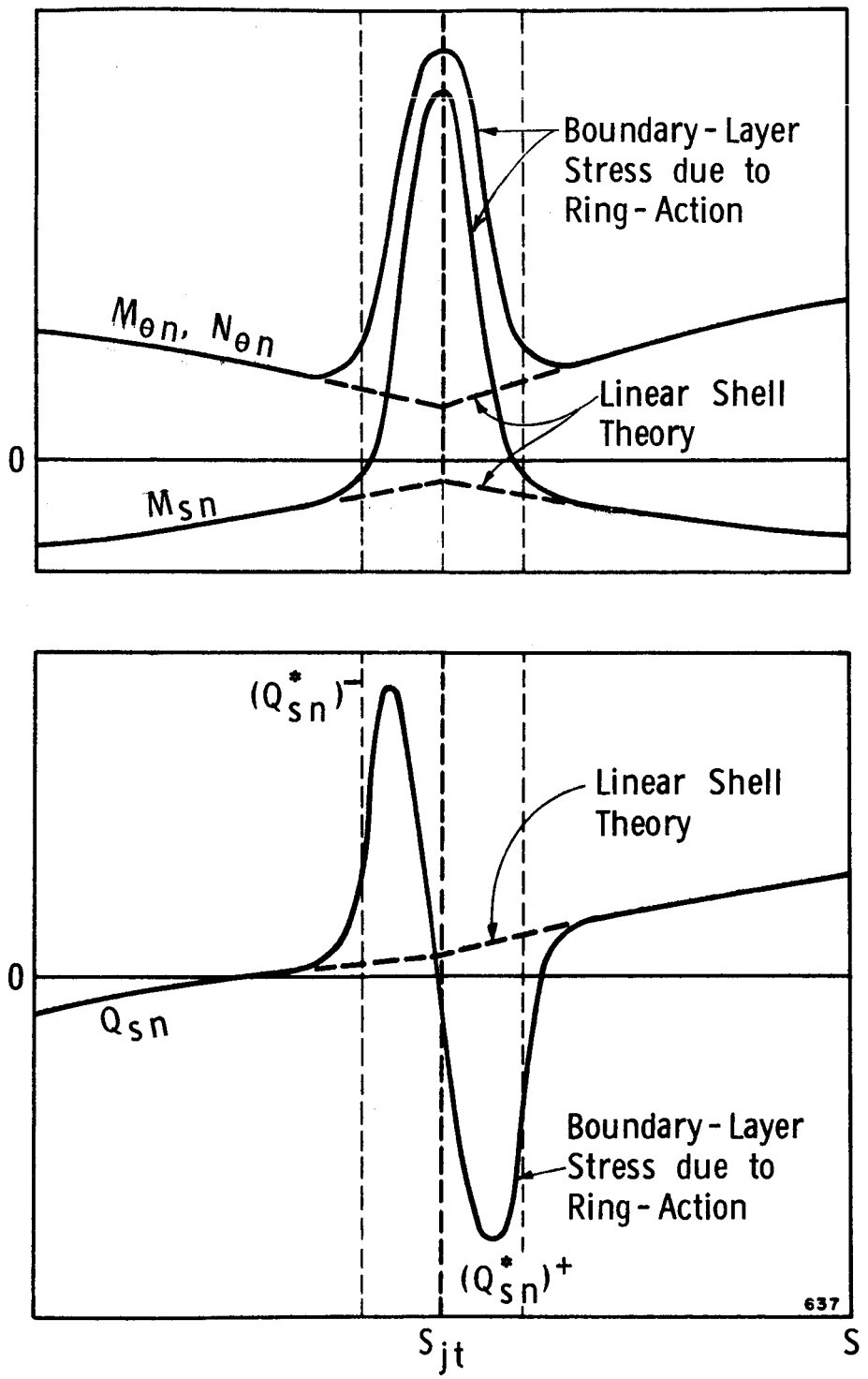

Figure 4. Boundary-Layer Stresses Due to "Ring-Action" of the Joint

shell vibration problem, in which an interior boundary-layer phenomenon must be analyzed.

It remains to mention that the large dynamic stresses induced near the joint add considerable importance to the problem. The local maximum stress near the joint may be several orders of magnitude greater than the stresses elsewhere, and may even reach the yield stress at relatively low amplitudes or under ordinarily safe dynamic environment. The vibratory or reversible nature of these boundary-layer stresses makes the joint especially vulnerable to possible material shake-down or fatigue.

EXPERIMENTAL APPARATUS AND PROCEDURE

Experiments were run on two shell models having the geometries described in Table 1. The experiments were similar to those described in Ref. 9 for conical shells. The essential features of the experiments are that the steel shells are driven by a pulsed magnetic field, and the transverse displacement is measured by a noncontacting probe. In this manner, neither the excitation nor the measuring system adds additional mass or stiffness to the thin shell.

TABLE 1

Model No.	α	$s_2 - s_1$	a	L	Boundary Condition
1	15°	13.57"	7.0"	21.0"	Freely supported
2	5°	11.15"	7.0"	11.15"	Clamped

The shell models were formed from 0.010-inch thick rolled steel shim stock. Both the conical and cylindrical components were formed from the flat sheet with one welded seam along a meridian. This seam was arc-welded with a butt-joint so that a negligible discontinuity was formed in the shell. The circular joint connecting the cone and the cylinder was similarly arc-welded and carefully ground to eliminate thickness change.

A photograph of the experimental apparatus and instrumentation is shown in Fig. 5. The shell models are supported from a mandrel of

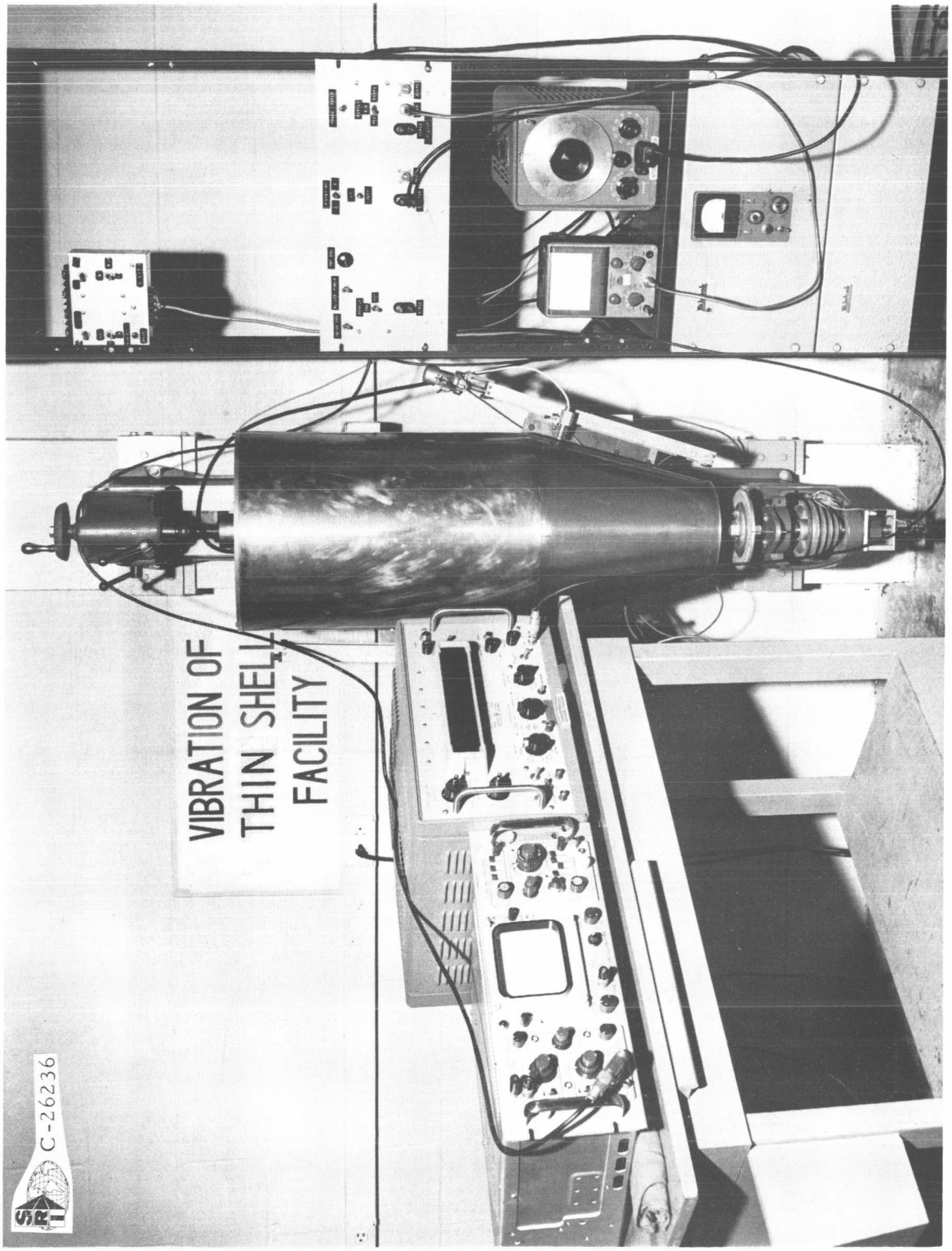

Figure 5. Experimental Set-Up

a vertically mounted lathe bed. The boundary support in Fig. 5 is that used to simulate the freely supported edge condition for Model No. 1. The right-angle groove in the circular plates supporting the upper and lower ends is machined to a close-tolerance fit with the edge of the shell. For Model No. 2, the edges of the shell were soldered into U-shaped grooves in the end plates to simulate the clamped boundary condition.

Excitation to the shells was produced by a pulsed magnetic field from four small electromagnets located at opposite ends of both a diameter of the conical shell and a diameter of the cylindrical shell, so that both shell components receive energy during resonance to compensate for damping, and the excitation of a normal mode is thus optimized by eliminating the reliance on energy transfer across the joint. The frequency of the excitation was controlled by an oscillator driving the electromagnets through a power amplifier. In order to optimize the excitation of each mode, a phase control is added so that the two pairs of electromagnets at opposite sides can be operated either in-phase or out-of-phase depending upon the circumferential wave number n being either even or odd. The position of the excitation along a meridian (s direction) of the shell is also adjustable so that various axial modes may be optimally excited.

The transverse displacement w is mapped with an inductance type displacement probe mounted on a long lead screw which can be adjusted to a position parallel to a generator either of the cone or of the cylinder. Thus,

the probe can traverse the shell in the s direction. The entire shell and excitation system may be rotated 360° on the central mandrel allowing a circumferential mode shape plot also. For direct plotting of the mode shapes, the position of the displacement probe with respect to the shell is given by a rotary potentiometer on the mandrel and a resistance slide wire on the lead screw assembly. The output signal from the displacement detector is conditioned through a tracking filter, tuned to the excitation frequency. The filtered output signal can be recorded on either an oscilloscope, frequency counter, or x-y pen recorder for mode shape plots.

Resonance is determined as the frequency at which maximum transverse amplitude response is observed on the oscilloscope. The accuracy of this method depends upon the sharpness of the amplitude-frequency response curves which, for low damping structures such as the shells tested, is sufficient to distinguish resonances separated by only a few cycles per second. Frequencies are read from an electronic frequency counter. Modes may be identified most easily by observing the phase relationship between the driving signal from the oscillator and the response signal from the displacement detector, both appear on the oscilloscope screen. Upon crossing a nodal line, the phase shifts 180° and is easily detected by the rotation of the Lissajous figure on the oscilloscope. Mode shapes can be plotted directly on an x-y pen recorder, with the rectified normal displacement amplitude on the y axis, and the circumferential or meridional position on the x axis.

EXPERIMENTAL RESULTS AND DISCUSSION

Resonant Frequencies

The resonant frequencies for the two composite shell models tested are presented graphically in Figs. 6 and 7. The measured frequency, in cps, is plotted against the circumferential wave number n, for the axial mode number m = 1 and 2.

For Model No. 1, the resonant frequencies are very close to the corresponding ones of the cylindrical component alone, with the joint considered as freely supported also. This is because the 15° cone is much shorter and stiffer (due to the taper) than the cylindrical component, and thus has relatively little motion during resonance compared to the cylinder. The solid curves in Fig. 6 are the calculated frequencies of the cylindrical component alone, considered as freely supported at both ends. The material parameters used in these calculations are $E = 30 \times 10^6$ psi, $\nu = 0.3$, and $\rho = 7.35 \times 10^{-4}$ lb $sec^2/in.^4$ We will discuss later the relationship of the mode shapes in the two cases.

If we examine the constraint that the cylindrical shell component feels at the joint, we find that there are two important changes from the idealized freely supported edge: (1) the conditions $w = 0$ is now partially released (see Fig. 8) which tends to lower the frequency; (2) the condition $N_s = 0$ is now partially restrained, thus there is a tendency to raise the frequency. From Fig. 6, we see that, for $n < 5$, the former has stronger

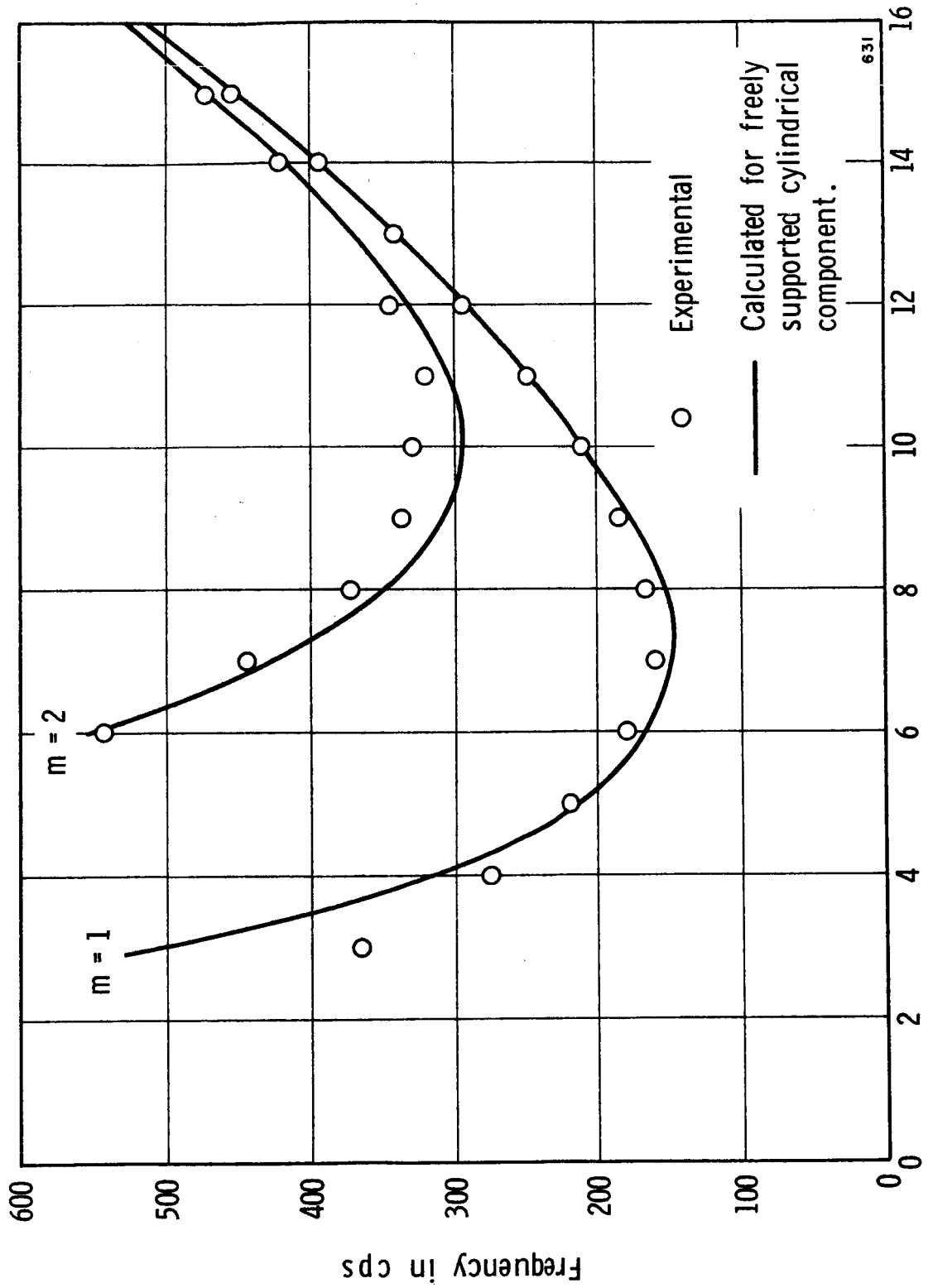

Figure 6. Resonant Frequencies of Model No. 1

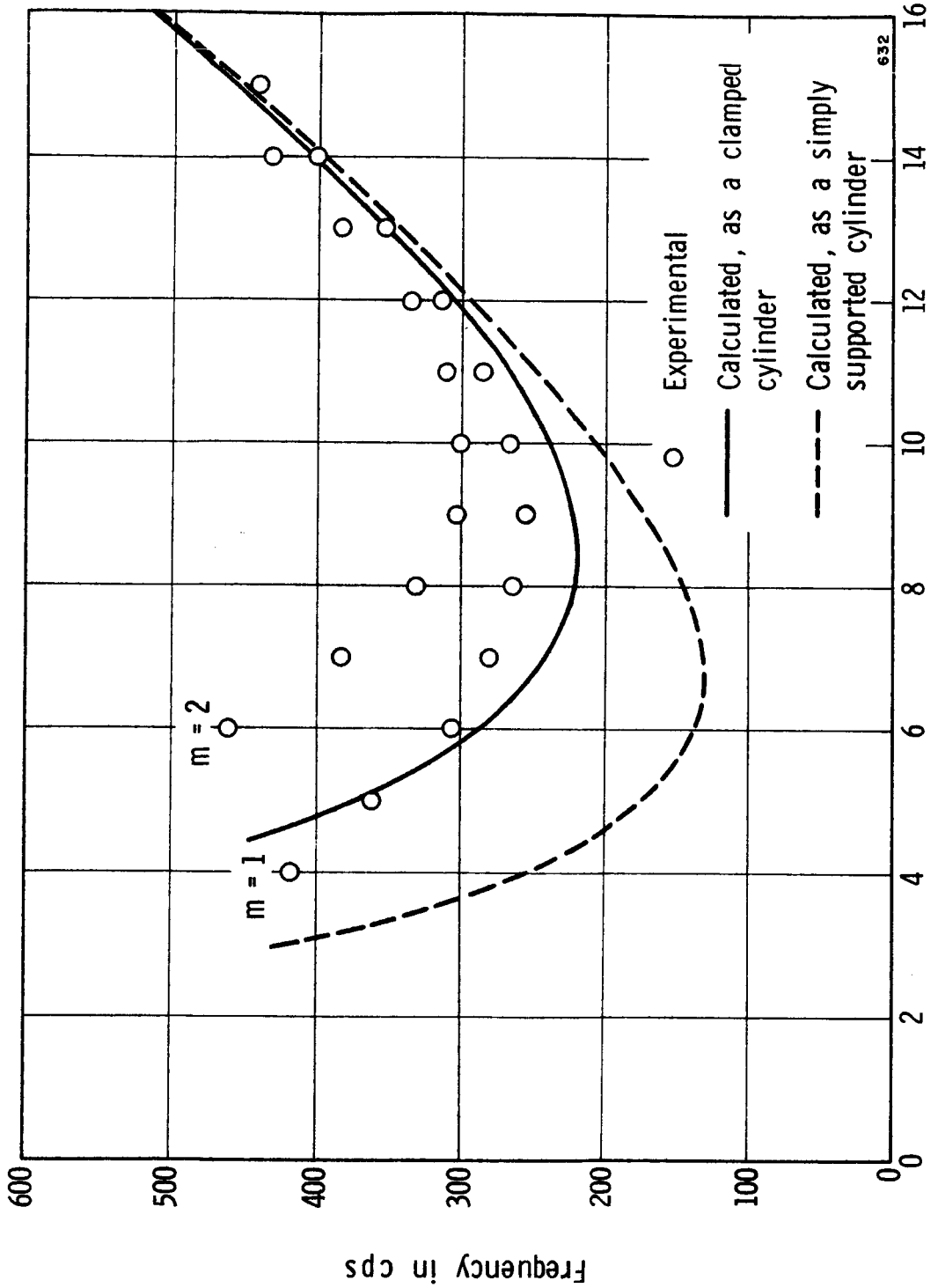

Figure 7. Resonant Frequencies of Model No. 2

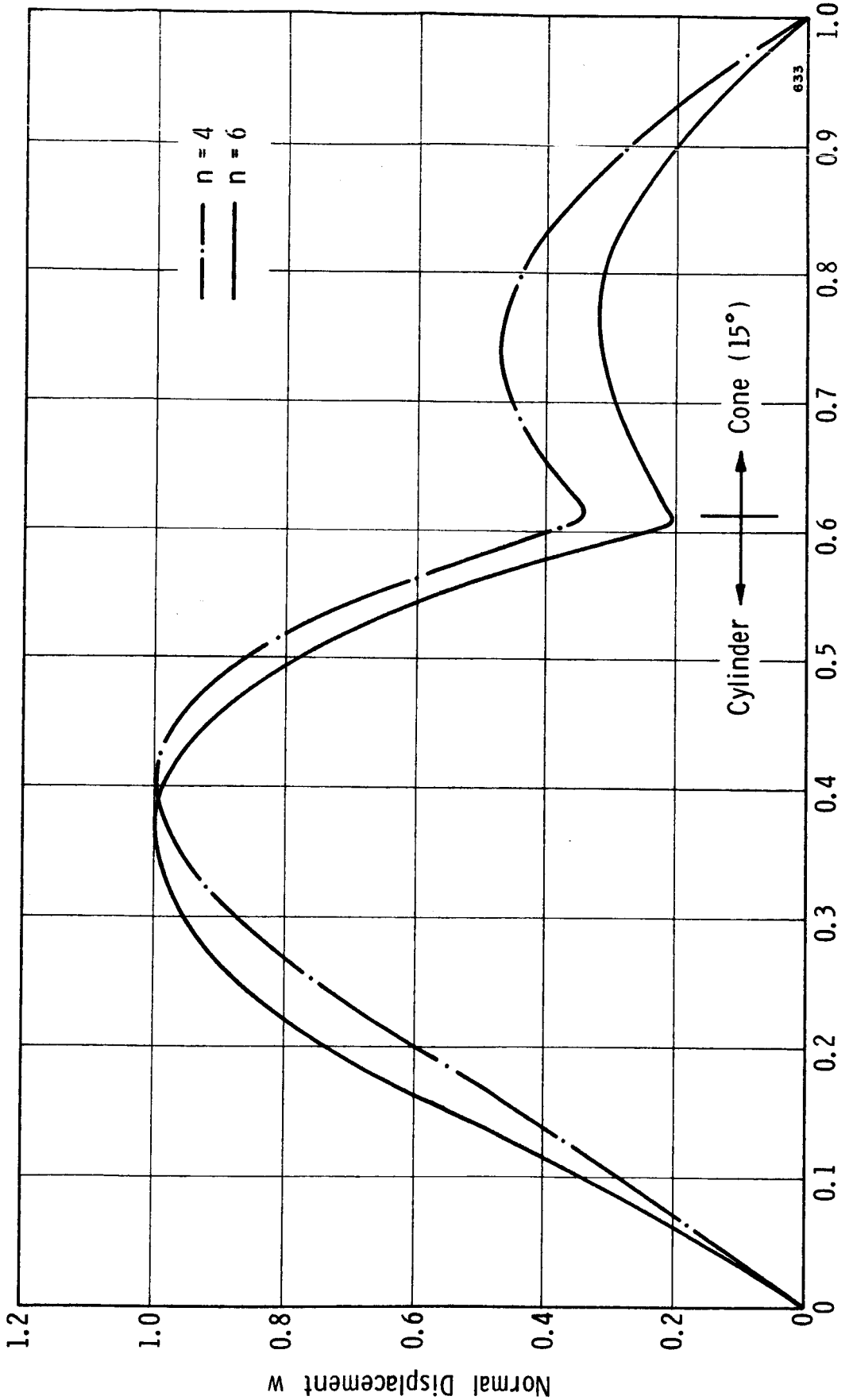

Figure 8. Meridional Mode Shape of Model No. 1

effects to cause an appreciable frequency decrease; for n = 5 ~ 9, the latter overshoots slightly; while for larger n, all effects become negligible. Similar observation can be made for m = 2.

Figure 7 shows the similar frequency plot for Model No. 2, which has a much weaker discontinuity (5° change in ϕ) at the joint. The two shell components are of the same height (11.15"), and therefore have nearly the same stiffness. The two edges of the composite shell were soldered to the end plates, as described before, to simulate the clamped boundary; however, since the shell is extremely thin (h/a = 0.00143) and the soldering material was softer than rolled steel, the resulting boundary condition is believed to lie somewhat between the clamped edge and the simply supported edge (with meridional constraint), as indicated by the mode shape plots (Figs. 9 and 10). For the interest of comparison, calculation was made for the theoretical frequencies of a clamped (solid curve in Fig. 7) and a simply supported (dashed curve in Fig. 7) cylindrical shell with the same total height as the model, but without the 5° taper. The calculation was made with a computer program utilizing the Fourier expansion method developed in Refs. 8 and 9. It is seen that the joint raises the frequencies as expected.

The frequency plots for both shells are characterized by having a minimum frequency for each axial mode number m, occurring at some value of n. This is similar to the behavior of the supported circular

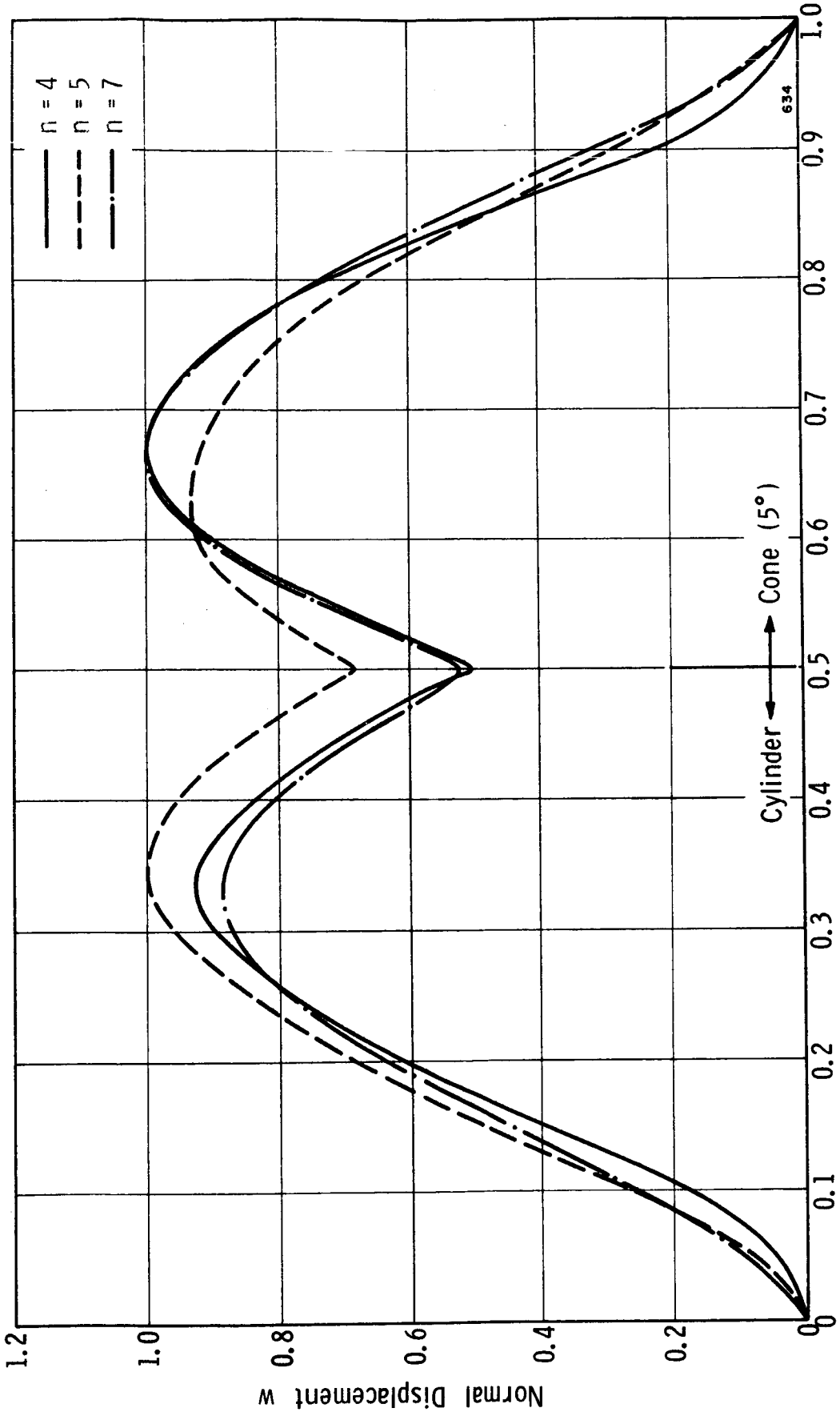

Figure 9. Meridional Mode Shape of Model No. 2

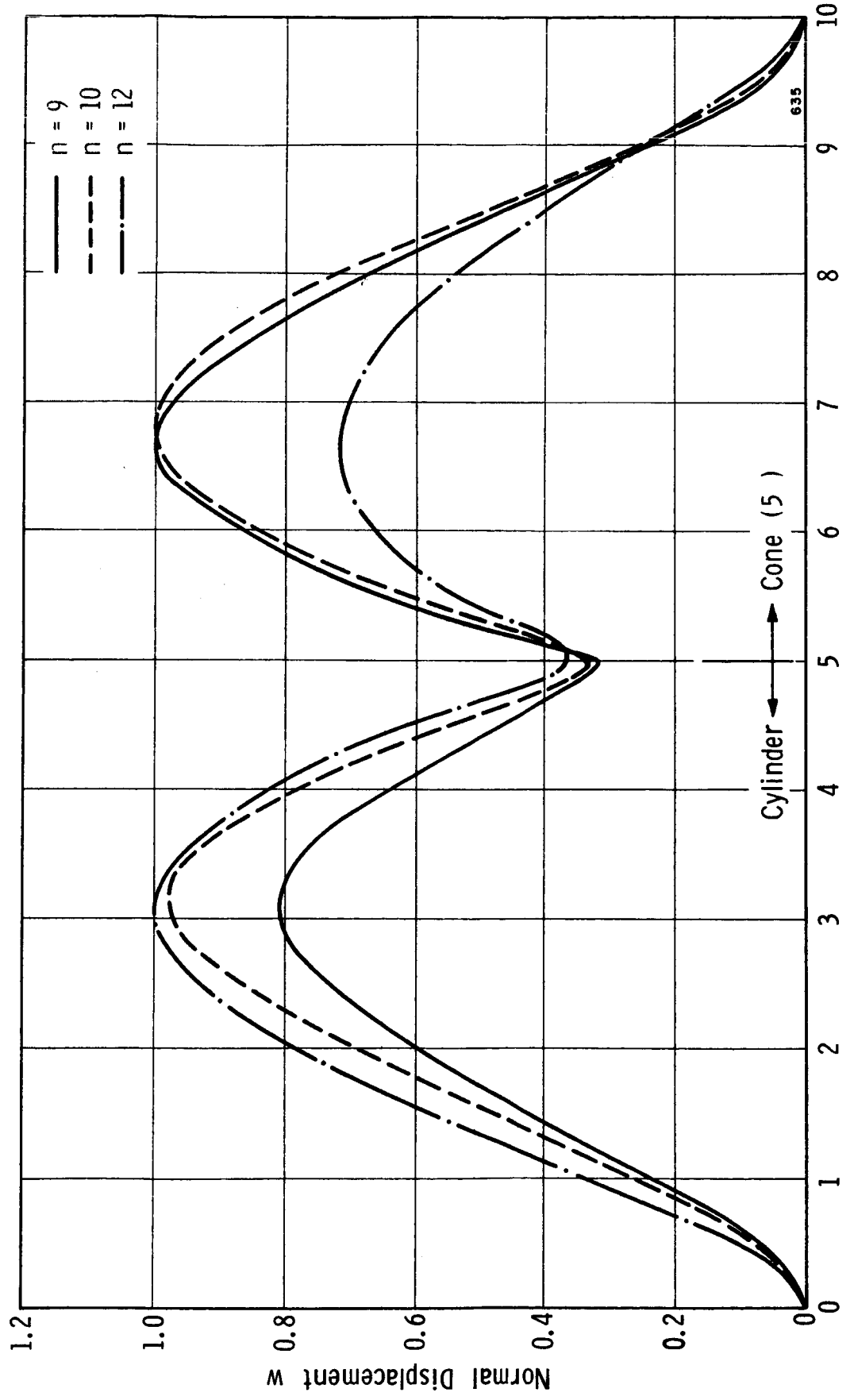

Figure 10. Meridional Mode Shape of Model No. 2

cylindrical shell, sometimes referred to as "Arnold-Warburton effect." The value of n at which the minimum frequency occurs is also dependent upon the geometric parameters of the shell, mainly the thickness ratio h/a. For low values of n, the frequency curve turns sharply upward because of the rapid increase of the membrane strain energy in this region. For large n (short wavelength), the strain energy is contributed predominantly by the bending stiffness of the shell.

We should emphasize that the high density of resonant frequencies and the increased stiffness at the joint often results in considerable difficulty in experimental separation of some neighboring modes and, in fact, difficulty in excitation of a pure normal mode at nearly all the resonances tested. It is difficult to make general statements about the frequency spectrum for composite shells, since it is influenced by so many factors.

Mode Shapes

The most striking feature disclosed in this modal vibration experiment of composite shells is probably the unexpected nonanalytical mode shapes in meridional direction, as plotted in Figs. 8 through 10. The V-shaped minimum of the w-s curve observed at the joint in all mode-shape mappings is a direct evidence of the "ring-action" discussed previously, and of the existence of a boundary-layer.

The circumferential mode shapes, however, appear to be proportional to sin $n\theta$ as expected. The nodal pattern, therefore, still consisted

of parallel circles and equispaced meridians as in simple axisymmetric shells. It should be emphasized that, for the second axial mode, m = 2, the middle nodal circle does not necessarily coincide with the joint. For Model No. 1, these middle nodal circles always occurred within the cylinder, while for Model No. 2, the exact position of the nodal circles was extremely difficult to determine, because of the difficulty in exciting a pure mode. But for this special shell geometry, the middle nodal circle is probably very close to the joint.

All the mode shape mappings for m = 1 have the same general appearance; therefore, only selected modes (for some n values) are presented. Figure 8 shows the typical meridional mode shape for Model No. 1. It is seen that the conical component has much less motion, and that the cylindrical component has a mode shape of nearly half sine wave — the mode shape for a freely supported cylinder. Therefore, for all practical purposes, the joint, together with the cone, may be considered roughly as a ring support in the calculation of resonant frequencies (solid curve in Fig 6). This conclusion applies, of course, only to cases when the conical component is relatively short and the cone angle sufficiently large.

Figures 9 and 10 show the typical meridional mode shapes of Model No. 2 for first axial modes. The transverse displacement w always has two nearly equal peaks, one in each shell component. The magnitude of

the displacement at the joint generally drops to less than half the peak displacement, forming a sharp valley. It is suspected that, for some cases when the amplitude is sufficiently large, a segment of "plastic hinge" may be developed at each antinode of the circular joint.

We might point out that the absolute accuracy of the mode shape mappings is rather poor. Also, the amplitude response at resonance does not appear to have any uniform progression with frequency or the circumferential mode number. These are mainly due to the previously mentioned difficulty in exciting a pure normal mode.

CONCLUSIONS

It is felt that the following conclusions may be justifiably made from the work presented.

1. Modal vibrations of axisymmetric composite shells present a unique problem in shell theory, with an unsolved analytical paradox and great experimental difficulties. A satisfactory solution of this problem hinges on a better understanding and analysis of the boundary-layer region enclosing the joint.

2. The meridional mode shape of a composite shell always contains a V-shaped minimum at the joint, with the local displacement amplitude greatly suppressed by the ring action of the joint.

3. Dynamic stress concentration will undoubtedly occur at the joint, even during free vibration of the shell. The use of a composite shell without reinforcement is not recommended for structures in any dynamic environment, in view of its vulnerability to crack formation.

4. The frequencies plotted against circumferential wave number n form a smooth curve for each axial mode number, with a minimum at some value of n, similar to the supported circular cylindrical shell.

5. The frequency spectrum is extremely dense. The transverse displacement response to foreign excitation is likely to be complicated, participated by a great number of modes.

ACKNOWLEDGEMENTS

The author wishes to acknowledge gratefully Dr. U. S. Lindholm for many valuable discussions and for his general support and encouragement in carrying out this program, Mr. J. F. Gormley for performing the experiments and computation, and Mr. T. R. Jackson for his assistance in the programming.

REFERENCES

1. Gros, C. G., and Forsberg, K., "Vibrations of Thin Shells: A Partially Annotated Bibliography," Lockheed Missiles and Space Company, Report SB-63-43 (1963).

2. Hu, W. C. L., "Survey of the Literature on the Vibrations of Thin Shells," Southwest Research Institute Project 02-1504, Tech. Rept. No. 1 (1964).

3. Kalnins, A., "Dynamic Problems of Elastic Shells," Applied Mechanics Reviews, 18, pp. 867-872 (1965).

4. Budiansky, B., and Radkowski, P. P., "Numerical Analysis of Unsymmetric Bending of Shells of Revolution," AIAA Journal, 1, pp. 1833-1842 (1963).

5. Kalnins, A., "Free Vibrations of Rotationally Symmetric Shells," J. Acous. Soc. Am., 36, pp. 1355-1365 (1964).

6. Cohen, G. A., "Computer Analysis of Asymmetric Free Vibrations of Orthotropic Shells of Revolution," AIAA Paper 65-109 (1965).

7. Saunders, H., and Paslay, P. R., "Inextensional Vibrations of a Sphere-Cone Shell Combination," J. Acous. Soc. Am., 31, pp. 579-583 (1959).

8. Hu, W. C. L., "Free Vibrations of Conical Shells," NASA TN D-2666 (1965).

9. Lindholm, U. S., and Hu, W. C. L., "Nonsymmetric Transverse Vibrations of Truncated Conical Shells," AIAA Symp. on Struc. Dyn. and Aeroelast., Boston, Mass., pp. 389-399 (1965) (to appear in Int. J. Mech. Sci.).